Research Article

Abdelraheem M. Aly*, Zehba Raizah, Hijaz Ahmed, Amal M. Al-Hanaya, and Noura Alsedias

# Double diffusion in a combined cavity occupied by a nanofluid and heterogeneous porous media

https://doi.org/10.1515/phys-2022-0189
received February 01, 2022; accepted July 14, 2022

**Abstract:** The aim of the present study is to simulate double diffusion in a circular cylinder over a rectangular cavity by utilizing incompressible smoothed particle hydrodynamics (ISPH) method. An originality of this study is adopting the ISPH method in simulating double diffusion in a novel domain of a circular cylinder over a rectangular shape occupied by $Al_2O_3$–$H_2O$ and heterogeneous porous media. The variations of Darcy parameter (Da) between $10^{-3}$ and $10^{-5}$ with two levels of porous media, ($0 \le \eta_1 = \eta_2 \le 1.5$), Rayleigh number ($10^3 \le \mathrm{Ra} \le 10^5$) with variable buoyancy ratio parameter ($0 \le N \le 2$), solid volume fraction $\phi$ between 0 and 0.05, and Lewis number ($10 \le \mathrm{Le} \le 40$) on the features of heat/mass transport as well as velocity field are discussed. It is found that the homogeneous porous medium reduces the temperature and concentration within a combined cavity. A decrease in Darcy parameter from $10^{-2}$ and $10^{-5}$ suppresses the maximum of a nanofluid velocity by 75% regardless the levels of porous media. An increase in parameters Ra and N enhances the heat and mass transmission, as well as the nanofluid velocity. Adding more concentration of nanoparticles until 5% reduces the nanofluid velocity. The variations of boundary conditions are acting effectively in changing the temperature and concentration circulations within a combined cavity. Besides, the variations of boundary conditions change the maximum of the velocity field by 86.9%.

**Keywords:** circular cylinder, double-diffusion, ISPH method, homogeneous/heterogeneous porous media, nanofluid

## 1 Introduction

Numerical simulations for heat/mass transport in several cavities are studied by refs. [1–3]. There are several applications of double diffusion in the porous cavities such as the design of solar cells, petroleum reservoirs, and nuclear wastes [4–8].

In recent years, there are many studies in thermal systems filled with porous media and nanofluid due to their applications in heat exchangers, copper foams in channels, and electronic cooling systems. Nguyen *et al.* [9] used the incompressible smoothed particle hydrodynamics (ISPH) method for examining the impacts of wavy interface for a porous-nanofluid layers on natural convection in an enclosure. Ataei-Dadavi *et al.* [10] reported an experimental examination on mixed convection in a vented cubical cavity. Nguyen *et al.* [11] studied ferro-nanofluid in a curved porous enclosure. Selimefendigil and Oztop [12] examined forced convection of a nanofluid in U-shaped cavity. The heat transfer for a ferrofluid with $Fe_3O_4$ nanoparticles in a trapezoidal cavity was numerically examined by Khan *et al.* [13]. Raja *et al.* [14] used a stochastic numerical scheme for nanofluidics of nonlinear Jeffery–Hamel flow. Raja *et al.* [15] utilized neural networks with Levenberg Marquardt technique to endorse the biconvection nanofluidic flow and Cattaneo-christov heat & mass flux on a permeable medium with considering the impacts of Darcy-Forchheimer law. More studies are introduced in ref. [16–23]. Ismael [24] studied the heat-mass transmission during mixed convection in a partially stratified porous enclosure. Numerical studies of natural convection in a partially stratified porous enclosure including an embedded solid conductive shape are introduced by Ismael and Ghalib [25].

Computational fluid dynamics method is significant in handling the thermal manner of the nanofluid flow through numerous simulations. Different numerical methods

* **Corresponding author: Abdelraheem M. Aly,** Department of Mathematics, College of Science, King Khalid University, P.O. Box 9004, 61413, Abha, Saudi Arabia; Department of Mathematics, Faculty of Science, South Valley University, 83523, Qena, Egypt, e-mail: abdelreheam.abdallah@sci.svu.edu.eg
**Zehba Raizah:** Department of Mathematics, College of Science, King Khalid University, P.O. Box 9004, 61413, Abha, Saudi Arabia
**Hijaz Ahmed:** Department of Basic Sciences, University of Engineering and Technology, Peshawar, Pakistan
**Amal M. Al-Hanaya, Noura Alsedias:** Department of Mathematical Sciences, College of Science, Princess Nourah bint Abdulrahman University, P.O.Box 84428, Riyadh 11671, Saudi Arabia

were used to solve several fluid dynamic problems. However, some new numerical technique like the ISPH have likewise been utilized to accomplish accurate engineering predictions. Utilizing the Galerkin finite element method (FEM), Kadhim *et al.* [26] investigated heat transfer of a hybrid nanofluid in cavity having opposing sinusoidal walls. The Lattice Boltzmann method was utilized by several researchers including Sheikholeslami *et al.* [27] to examine magnetohydrodynamic-free convection in a cubic cavity including a hot sphere. Seyyedi *et al.* [28] adopted the control volume FEM (CVFEM) to study the entropy generation and free convection flow of nanoencapsulated phase change materials (NEPCMs) within a porous annulus. Also, the NEPCMs inside $n$ elliptical-shaped enclosure under magnetic field effects are studied numerically using CVFEM by Seyyedi *et al.* [29]. Hashemi-Tilehnoee *et al.* [30] adopted finite volume method using ANSYS Fluent to examine the diluted NEPCM inside a water-filled a hot enclosure. Seyyedi [31] utilized CVFEM for entropy generation analysis and free convection within a cardioid shaped porous cavity. The ISPH method was introduced by Aly Abdelraheem [32] to examine natural convection of a heated obstacle within a circular domain. Further studies of the ISPH method in several problems of the CFD can be found in refs. [33–37]. Raizah *et al.* [38] utilized ISPH method for studying impacts of thermal diffusion and diffusion-thermo on the transport of heat and mass of a nanofluid inside an annulus including three circular cylinders.

The novelty of this study is checking thermosolutal convection in a novel shape of a circular cylinder over rectangular domain by using the ISPH method. The problem of heat transfer and fluid flow within a porous combined domain of a circular cylinder over a rectangular shape can be applied in air crafting, electronic devices, cooling of a nuclear and power plant, and heat exchangers tubes. The combined domain is mobilized by a nanofluid ($Al_2O_3$–$H_2O$) and homogeneous/heterogeneous porous media. By comparison between the heterogeneous and homogeneous porous media, it is found that a homogeneous porous medium reduces heat and mass transport and nanofluid velocity inside a combined cavity. Further, the homogeneous porous level provides more stable movements of the nanofluid flow within a combined domain of a circular cylinder over a rectangular shape compared to a heterogeneous porous level. Regardless of the porous level, a reduction in Da reduces the nanofluid movements due to the low permeability. Increasing Ra and $N$ strengthens the buoyancy forces that support the mass/heat transfer and augments the nanofluid movements within a combined cavity. Average Nusselt number $\overline{\mathrm{Nu}}$ is enhanced at a heterogeneous porous medium, while average Sherwood number $\overline{\mathrm{Sh}}$ is enhanced at a homogeneous porous medium. We hope that this work serves in the forthcoming investigation of adjusting thermal transport within closed complex domains.

## 2 Mathematical formulations

Figure 1 indicates the primary physical and mesh generation diagrams. The model contains a circular cylinder over a rectangular-shaped cavity. The length of a rectangular shape is $L = 1.0$ and width 0.4, and a radius of upper circular cylinder is $R_c = 0.5$. The surface of the circular cylinder has $T_h$ and $C_h$. The normal walls of a rectangular shape have adiabatic boundary conditions,

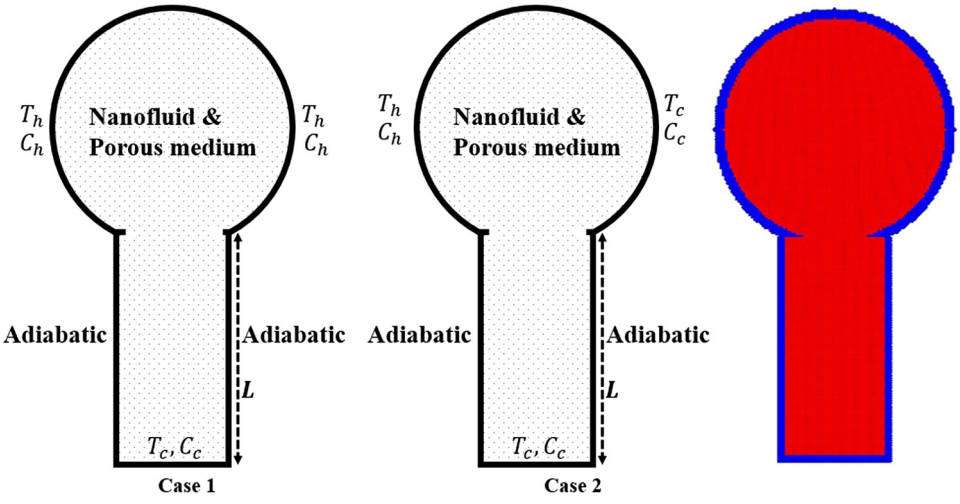


**Figure 1:** Primary physical diagram and mesh generation models.

**Table 1:** $Al_2O_3$–$H_2O$ characteristics

| | $\rho$ (Kg/m³) | $K$ (W/m K) | Cp (J/kg K) | $\beta \times 10^{-5}$ (1/K) | $d$ (nm) |
|---|---|---|---|---|---|
| $Al_2O_3$ | 3,970 | 40 | 765 | 0.85 | 33 |
| Water | 993 | 0.628 | 4,178 | 36.2 | 0.385 |

and the plane wall has $T_c$ and $C_c$. The combined cavity of a circular cylinder over a rectangular shape is occupied with $Al_2O_3$–$H_2O$ and heterogeneous/homogeneous porous media. The time-dependent flow is laminar and incompressible. Table 1 introduces the characteristics of $Al_2O_3$–water.

Time-dependent thermosolutal convection of nanofluid in a combined cavity suspended by a heterogeneous porous medium according to ref. [39] is expressed as follows:

$$\frac{\partial V}{\partial Y} = -\frac{\partial U}{\partial X}, \tag{2.1}$$

$$\frac{1}{\varepsilon}\frac{\mathrm{d}U}{\mathrm{d}\tau} = -\frac{\partial P}{\partial X} + \frac{\rho_f}{\rho_{nf}}\left(\frac{1}{\varepsilon}\frac{\partial}{\partial X}\left(\mathrm{Pr}\frac{\mu_{nf}}{\mu_f}\frac{\partial U}{\partial X}\right) + \frac{1}{\varepsilon}\frac{\partial}{\partial Y}\left(\mathrm{Pr}\frac{\mu_{nf}}{\mu_f}\frac{\partial U}{\partial Y}\right) - \frac{\mathrm{Pr}\mu_{\mathrm{eff}}}{\mu_{nf}K^*(X,Y)\mathrm{Da}}U\right), \tag{2.2}$$

$$\frac{1}{\varepsilon}\frac{\mathrm{d}V}{\mathrm{d}\tau} = \frac{\rho_f}{\rho_{nf}}\left(\frac{1}{\varepsilon}\frac{\partial}{\partial X}\left(\mathrm{Pr}\frac{\mu_{nf}}{\mu_f}\frac{\partial V}{\partial X}\right) + \frac{1}{\varepsilon}\frac{\partial}{\partial Y}\left(\mathrm{Pr}\frac{\mu_{nf}}{\mu_f}\frac{\partial V}{\partial Y}\right) - \frac{\mathrm{Pr}\mu_{\mathrm{eff}}}{\mu_{nf}K^*(X,Y)\mathrm{Da}}V + \frac{(\rho\beta)_{nf}}{(\rho\beta)_f}\mathrm{PrRa}\theta\right) - \frac{\partial P}{\partial Y}, \tag{2.3}$$

$$\gamma\frac{\mathrm{d}\theta}{\mathrm{d}\tau} = \frac{(\rho c_p)_f}{(\rho c_p)_{nf}}\left[\frac{\partial}{\partial X}\left(\zeta(X,Y)\frac{\partial\theta}{\partial X}\right) + \frac{\partial}{\partial Y}\left(\zeta(X,Y)\frac{\partial\theta}{\partial Y}\right)\right], \tag{2.4}$$

$$\frac{\mathrm{d}\Phi}{\mathrm{d}\tau} = \frac{1}{\mathrm{Le}}\left[\frac{\partial}{\partial X}\left(\Pi(X,Y)\frac{\partial\Phi}{\partial X}\right) + \frac{\partial}{\partial Y}\left(\Pi(X,Y)\frac{\partial\Phi}{\partial Y}\right)\right]. \tag{2.5}$$

Here, the definitions of a porous matrix are expressed as follows:

$$K^* = e^{\eta_1 HX + \eta_2 HY}, \tag{2.6}$$

$$\zeta = \varepsilon\frac{k_{nf}}{k_f} + (1-\varepsilon)e^{\eta_1 HX + \eta_2 HY}, \tag{2.7}$$

$$\Pi = \frac{D_{\mathrm{eff}}}{D_0} = \frac{D_0 e^{\eta_2 HY + \eta_1 HX}}{D_0}, \tag{2.8}$$

$$\gamma = (\varepsilon(\rho c_p)_{nf} + (1-\varepsilon)(\rho c_p)_p)((\rho c_p)_{nf})^{-1}. \tag{2.9}$$

The physical definitions of a nanofluid according to refs. [40–42] are given as follows:

$$\rho_{nf} = (1-\phi)\rho_f + \phi\rho_p, \tag{2.10}$$

$$\alpha_{nf} = k_{nf}((\rho c_p)_{nf})^{-1}, \tag{2.11}$$

$$(\rho\beta)_{nf} = (1-\phi)(\rho\beta)_f + \phi(\rho\beta)_p, \tag{2.12}$$

$$(\rho c_p)_{nf} = (1-\phi)(\rho c_p)_f + \phi(\rho c_p)_p, \tag{2.13}$$

$$\mu_{nf} = \mu_f \Big/ \left(-34.87\left(\frac{d_p}{d_f}\right)^{-0.3}\varphi^{1.03} + 1\right), \tag{2.14}$$

$$k_{nf} = \left(4.4(\mathrm{Re}_B)^{0.4}\,\mathrm{Pr}^{0.66}\left(\frac{T}{T_{rf}}\right)^{10}\left(\frac{k_p}{k_f}\right)^{0.03}\varphi^{0.66} + 1\right)k_f, \tag{2.15}$$

$$\mathrm{Re}_B = \frac{\rho_f u_B d_p}{\mu_f}, \tag{2.16}$$

$$u_B = \frac{2K_B T}{(\pi\mu_f d_p^2)}, \tag{2.17}$$

where $T_{rf}$ is a freezing point. Boltzmann's factor $K_B = 1.380648 \times 10^{-23}$ J/K .

Average Sherwood $\overline{\mathrm{Sh}}$ and Nusselt $\overline{\mathrm{Nu}}$ numbers on a circular cylinder wall are defined as follows:

$$\overline{\mathrm{Sh}} = -\frac{1}{s}\int_0^s \frac{\partial\Phi}{\partial n}\mathrm{d}Y, \tag{2.18}$$

$$\overline{\mathrm{Nu}} = -\frac{1}{s}\int_0^s \frac{\partial(\zeta(X,Y)\theta)}{\partial n}\mathrm{d}Y. \tag{2.19}$$

# 3 Proposed methodology

The solving steps:

Predictor step:

$$U^* = \varepsilon\frac{\rho_f}{\rho_{nf}}\Delta\tau\left(\frac{1}{\varepsilon}\frac{\partial}{\partial X}\left(\mathrm{Pr}\frac{\mu_{nf}}{\mu_f}\frac{\partial U}{\partial X}\right) + \frac{1}{\varepsilon}\frac{\partial}{\partial Y}\left(\mathrm{Pr}\frac{\mu_{nf}}{\mu_f}\frac{\partial U}{\partial Y}\right) - \frac{\mathrm{Pr}\mu_{\mathrm{eff}}}{\mu_{nf}K^*(X,Y)\mathrm{Da}}U\right)^n + U^n, \tag{3.1}$$

$$V^* = \varepsilon\frac{\rho_f}{\rho_{nf}}\Delta\tau\left(\frac{1}{\varepsilon}\frac{\partial}{\partial X}\left(\mathrm{Pr}\frac{\mu_{nf}}{\mu_f}\frac{\partial V}{\partial X}\right) + \frac{1}{\varepsilon}\frac{\partial}{\partial Y}\left(\mathrm{Pr}\frac{\mu_{nf}}{\mu_f}\frac{\partial V}{\partial Y}\right) - \frac{\mathrm{Pr}\mu_{\mathrm{eff}}}{\mu_{nf}K^*(X,Y)\mathrm{Da}}V + \frac{(\rho\beta)_{nf}}{(\rho\beta)_f}\mathrm{PrRa}\theta\right)^n + V^n. \tag{3.2}$$

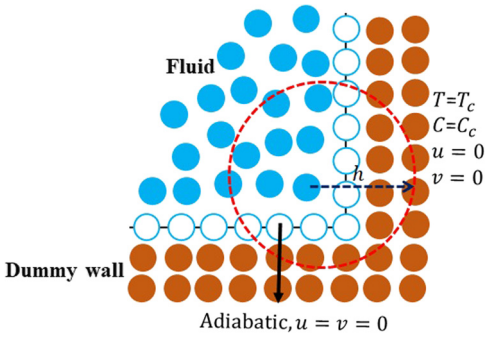


**Figure 2:** Dummy boundary particles of the ISPH method.

**Table 2:** $\overline{\text{Nu}}$ for various particle sizes $d_0$ at Le = 20, $N = 2$, $\varepsilon = 0.6$, Ra = $10^4$, and $\phi = 0.01$

| Grid | $d_0 = 0.02$ | $d_0 = 0.01$ | $d_0 = 0.005$ |
|---|---|---|---|
| $\overline{\text{Nu}}$ | 0.1124 | 0.1138 | 0.1143 |

Pressure Poisson equation:

$$\nabla^2 P^{n+1} = \alpha \frac{\rho - \rho^{num}}{\Delta\tau^2} + \frac{\rho}{\Delta\tau}\left(\frac{\partial U^*}{\partial X} + \frac{\partial V^*}{\partial Y}\right). \tag{3.3}$$

Relaxation factor $\alpha$ is between 0 and 1.

Corrected velocities:

$$U^{n+1} = -\frac{\Delta\tau}{\rho}(\nabla P^{n+1}) + U^*, \tag{3.4}$$

$$V^{n+1} = -\frac{\Delta\tau}{\rho}(\nabla P^{n+1}) + V^*. \tag{3.5}$$

Thermal energy equation:

$$\theta^{n+1} = \Delta\tau \frac{(\rho c_p)_f}{(\rho c_p)_{nf}} \times \left[\frac{\partial}{\partial X}\left(\zeta(X,Y)\frac{\partial\theta}{\partial X}\right) + \frac{\partial}{\partial Y}\left(\zeta(X,Y)\frac{\partial\theta}{\partial Y}\right)\right]^n + \theta^n \tag{3.6}$$

Concentration equation:

$$\Phi^{n+1} = \Delta\tau \frac{1}{\text{Le}} \times \left[\frac{\partial}{\partial X}\left(\Pi(X,Y)\frac{\partial\Phi}{\partial X}\right) + \frac{\partial}{\partial Y}\left(\Pi(X,Y)\frac{\partial\Phi}{\partial Y}\right)\right]^n + \Phi^n. \tag{3.7}$$

The positions:

$$X^{n+1} = \Delta\tau U^{n+1} + X^n \tag{3.8}$$

$$Y^{n+1} = \Delta\tau V^{n+1} + Y^n. \tag{3.9}$$

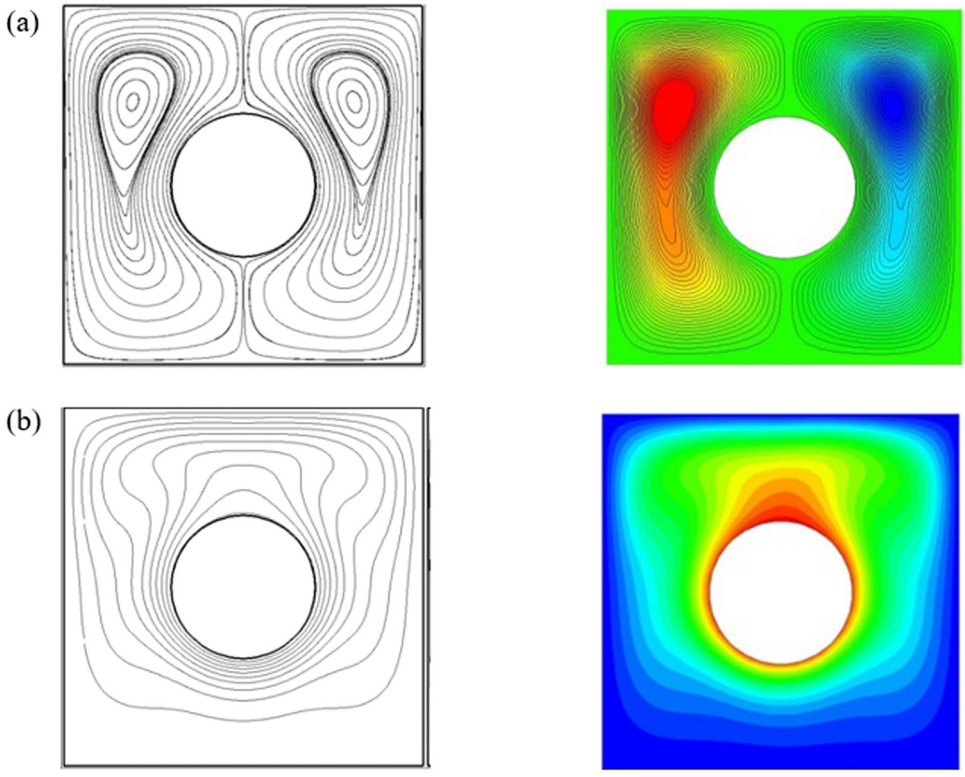


**Figure 3:** Streamlines and isotherms of Kim *et al.* [43] (left) and the ISPH data (right).

The shifting technique:

$$\Upsilon_{i'} = (\nabla \Upsilon)_i \delta R_{ii'} + \Upsilon_i + o\left(\delta R_{ii'}^2\right). \tag{3.10}$$

## 3.1 Boundary treatment

The dummy particles are utilized for treating the rigid walls. Dummy particles are settled uniformly around the cavity walls. Figure 2 displays the initial distributions of dummy particles. Dummy particles are utilized in preventing the error of a cut kernel.

## 3.2 Validation tests

To examine the grid independence of the ISPH method, Table 2 presents $\overline{\mathrm{Nu}}$ for various particle sizes $d_0$ at Ra = $10^4$, Le = 20, $\varepsilon$ = 0.6, $N$ = 2, and $\phi$ = 0.01. In Table 2, there is a slight difference on $\overline{\mathrm{Nu}}$ when changing $d_0$. Therefore, the medium size $d_0$ = 0.01 is selected.

To present the efficiency of the ISPH method, the numerical test of natural convection of an inserted hot source is introduced for the streamlines and isotherms by Kim *et al.* [43]. Figure 3 presents the streamlines and

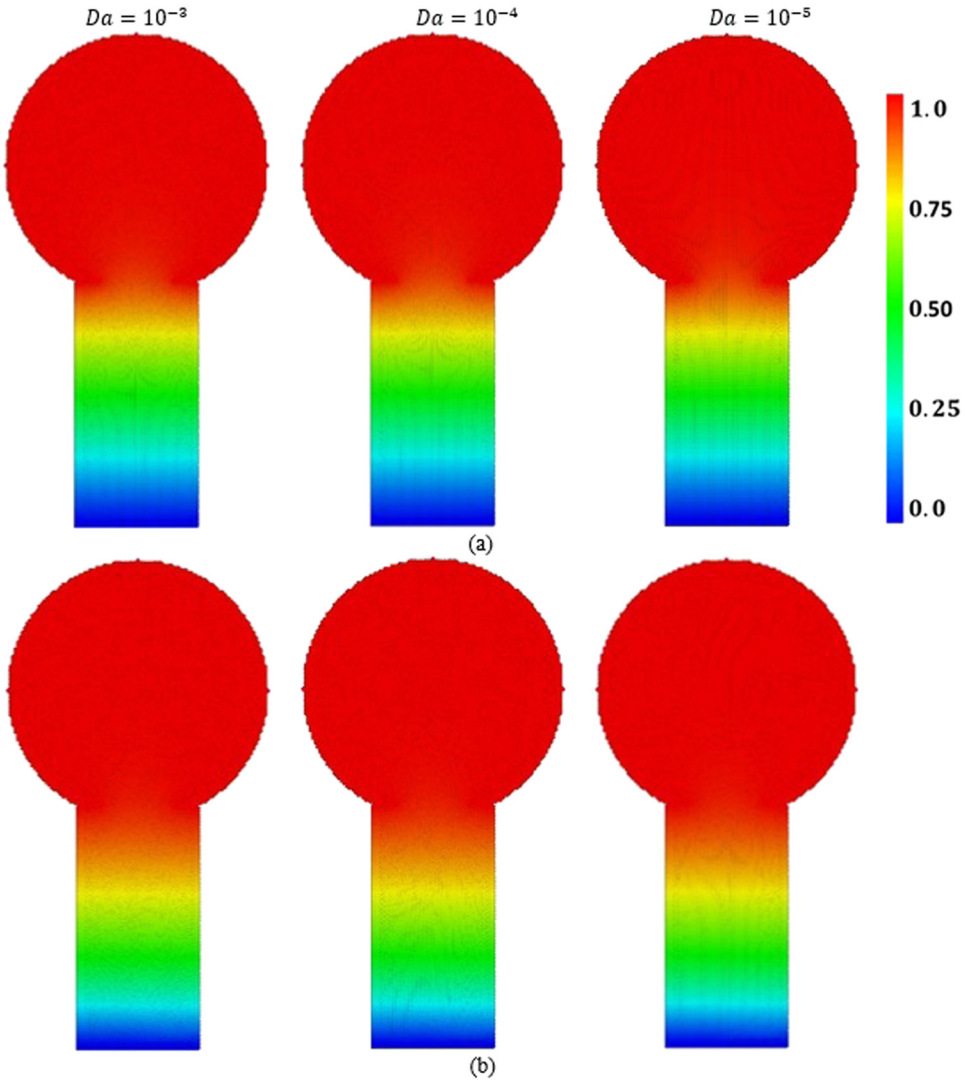


**Figure 4:** Varied Da with changing porous levels on temperature at $N$ = 1, $R_c$ = 0.1, Ra = $10^4$, $L_h$ = 0.25, $\phi$ = 0.01, and Le = 20. (a) Homogeneous porous media ($\eta_1 = \eta_2 = 0$). (b) Heterogeneous porous media ($\eta_1 = \eta_2 = 1.5$).

isotherms of an inserted hot source in a cavity. The ISPH method agrees well with the reference data of ref. [43].

## 4 Results and discussions

The numerical simulations represented in temperature, concentration, and velocity field below the influences of pertinent parameters are discussed in this section. The porosity of a porous medium is taken as $\varepsilon = 0.6$. Figures 4–6 present the effects of (Da) with two levels of porous media in the temperature, concentration, and velocity field. In Figure 4, it is seen that a decrease in Da augments the temperature allotments inside a combined cavity of a circular cylinder over a rectangular shape. A heterogeneous porous medium, $\eta_1 = \eta_2 = 1.5$, gives little higher temperature allotments compared to a homogeneous porous medium $\eta_1 = \eta_2 = 0$. In Figure 5, the concentration allotments are higher at a heterogeneous porous medium compared to a homogeneous porous medium. Moreover, a decrease in Da reduces the concentration allotments inside a combined cylinder-rectangular shaped cavity. In Figure 6, the maximum of velocity field decreases by 75% as Da reduces from $10^{-2}$ to $10^{-5}$ regardless the level of porous media. Besides, there are variations on the nanofluid movements between the homogeneous and heterogeneous porous media. The reason returns to the difference on the porosity of the porous media related to their level as a homogeneous or heterogeneous. It is

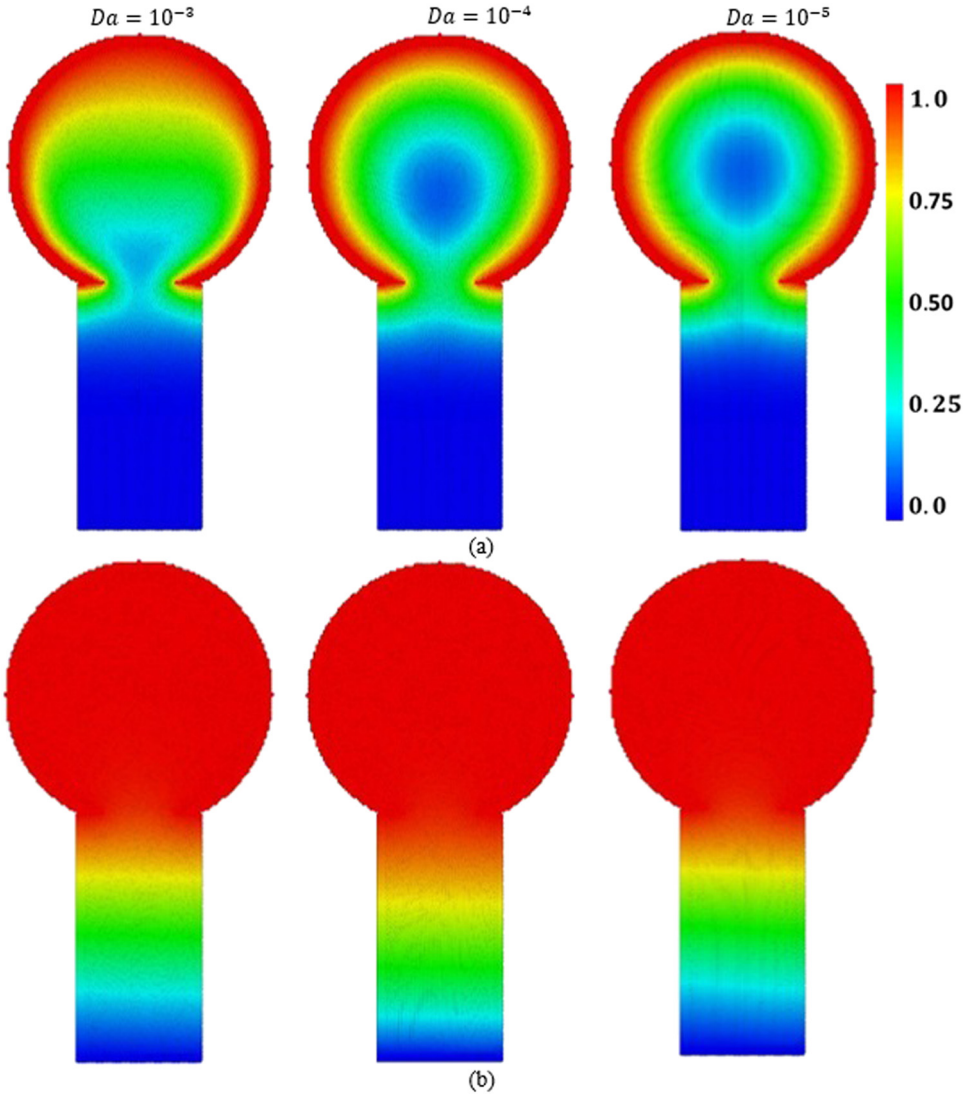


**Figure 5:** Varied Da with changing porous levels on concentration at $N = 1$, $R_c = 0.1$, $\mathrm{Ra} = 10^4$, $L_h = 0.25$, $\phi = 0.01$, and $\mathrm{Le} = 20$. (a) Homogeneous porous media ($\eta_1 = \eta_2 = 0$). (b) Heterogeneous porous media ($\eta_1 = \eta_2 = 1.5$).

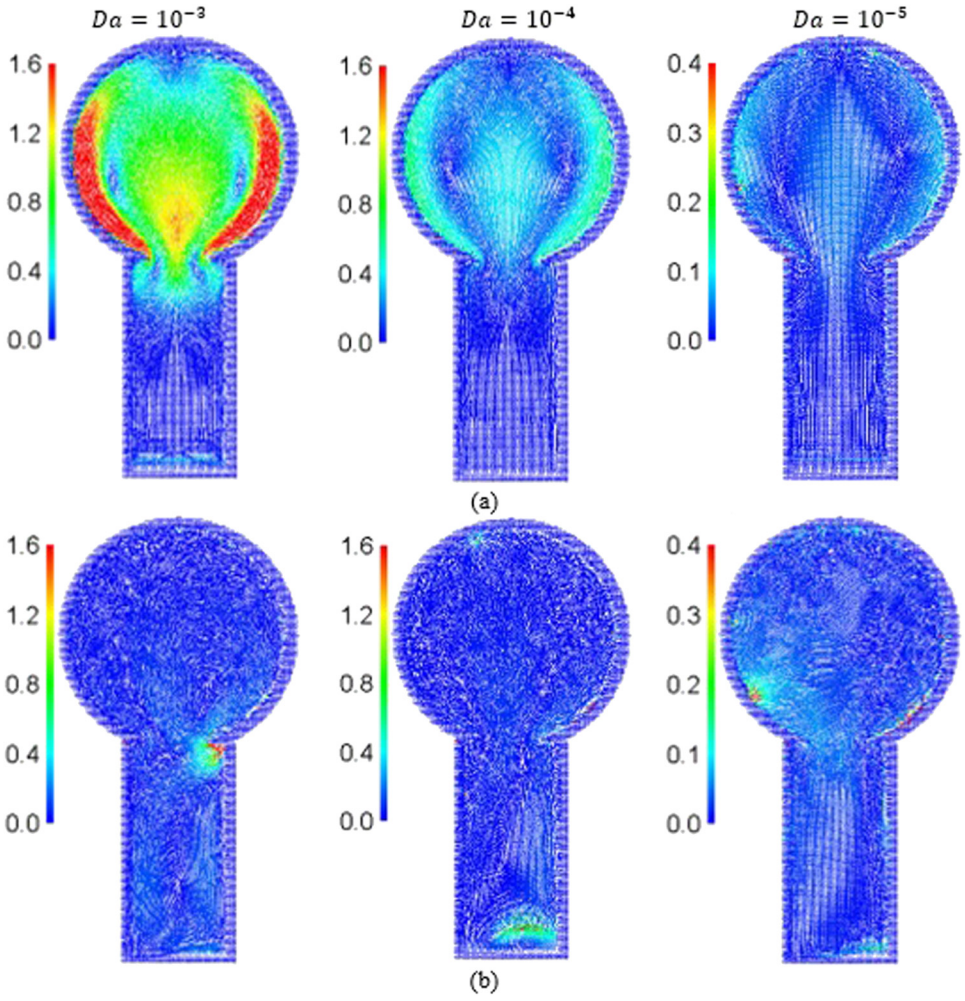


**Figure 6:** Varied Da with changing porous levels on velocity fields at $N = 1$, Ra $= 10^4$, $R_c = 0.1$, $L_h = 0.25$, $\phi = 0.01$, and Le $= 20$. (a) Homogeneous porous media ($\eta_1 = \eta_2 = 0$). (b) Heterogeneous porous media ($\eta_1 = \eta_2 = 1.5$).

found that the homogeneous porous media supports much stable nanofluid movements inside a combined domain compared to the heterogeneous porous media.

Figures 7 and 8 depict the influences of Ra with changing $N$ on concentration and nanofluid motion. Physically, the power of Ra and $N$ boosts the convection flows that accelerate the nanofluid movements and double diffusion. Besides, the direction of the nanofluid flow is dramatically influenced by the variations of $N$. In Figure 7, an augmentation in Ra provides an enhancement in the concentration distributions. Besides, an increase in $N$ augments concentration distributions. In Figure 8, as a result of a high buoyancy force at extra Ra, the nanofluid velocity accelerates as Ra boosts. An increase in $N$ augments the velocity field regardless of the values of Ra.

The effects of adding nanoparticles in features of heat/mass transport and velocity fields have been shown in Figures 9–11. In Figures 9 and 10, an increase in $\phi$ has a slight enhancement in the temperature and concentration circulations. The physical meaning is due to the high temperature/concentration in the top cylinder walls, which shrinks the contributions of $\phi$. In Figure 11, as $\phi$ augments the viscosity of the mixture fluid and hence, the velocity of a nanofluid decreases as $\phi$ increases. To prevent the solidifications between the porous media and nanofluid, the value of $\phi$ is limited to 5%.

The impacts of Lewis number Le on the heat/mass transfer and velocity field have been shown in Figures 12–14. In Figure 12, an increment in Le has a slight decrease in the temperature circulations. In Figure 13, increasing Le reduces the distributions of the concentration within a combined cylinder-rectangular cavity. In Figure 14, an increase in Le augments the nanofluid's velocity inside a combined cylinder-rectangular cavity.

Figures 15–17 present the thermal, mass patterns, and velocity field under changing boundary conditions of

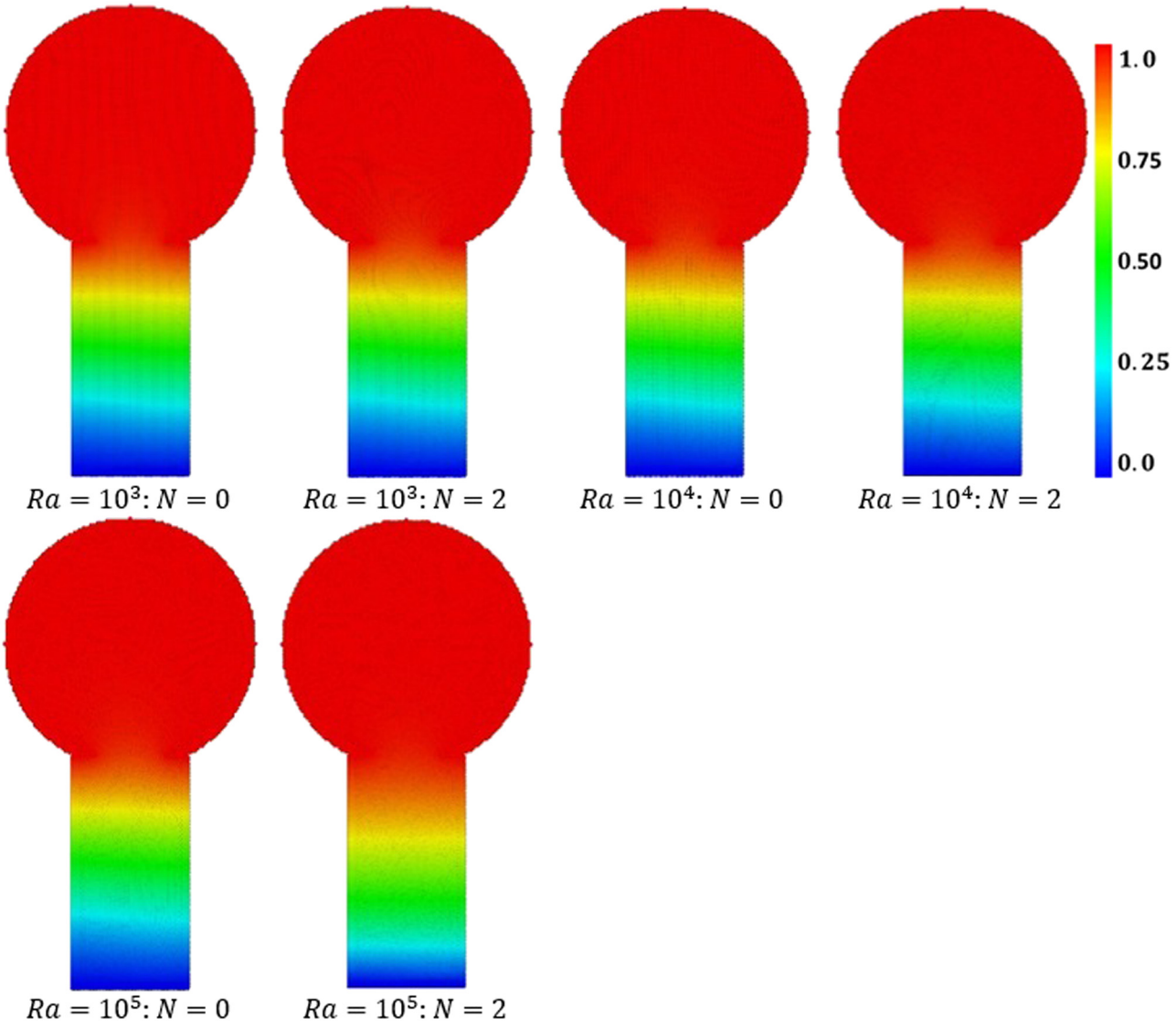


**Figure 7:** Variation of Ra with $N$ on concentration at $\eta_1 = \eta_2 = 1.5$, $L_h = 0.25$, $\phi = 0.01$, Da $= 10^{-3}$, and Le $= 20$.

a circular cylinder. In Figures 15 and 16, there are clear differences in the temperature and concentration patterns according to a change in circular cylinder boundary conditions. At case 1, a cylinder-wall has $T_h$, $C_h$, the thermal-solutal convection is highly increasing through the whole cavity. When the boundary condition of a circular cylinder became half $T_h$, $C_h$, and half $T_c$, $C_c$, (case 2), the thermal/solutal convection is shrinking into a half of a cavity. In Figure 17, the maximum of the velocity field reduces by 86.9% as the boundary condition of a circular cylinder changes from case 2 into case 1.

Figure 18 shows $\overline{\text{Nu}}$ and $\overline{\text{Sh}}$ along a circular cylinder wall below the effects of Da with two levels of porous media. $\overline{\text{Nu}}$ has lower values at a homogeneous porous medium compared to a heterogeneous porous medium. However, $\overline{\text{Sh}}$ has lower values at a heterogeneous porous medium. Moreover, a decrease in Da boosts the values of $\overline{\text{Nu}}$.

## 5 Conclusion

In this study, the double diffusion within a combined cavity of a circular cylinder over rectangular shape filled with $Al_2O_3$-water and a heterogeneous/homogeneous porous medium was examined numerically by the ISPH method. The variations of buoyancy ratio with Rayleigh number, various boundary conditions, solid volume fraction, Lewis number, and two levels of the porous media with

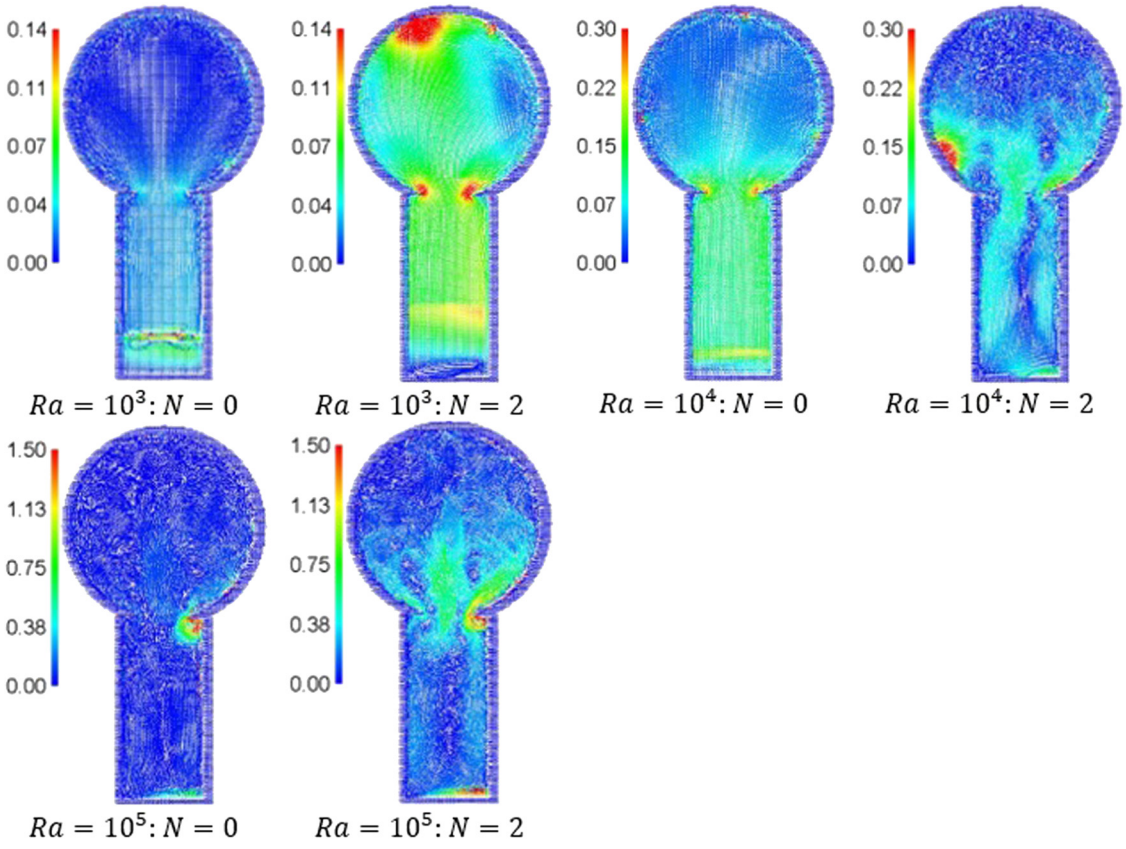


**Figure 8:** Variation of Ra with $N$ on velocity field at $\eta_1 = \eta_2 = 1.5$, Da $= 10^{-3}$, $L_h = 0.25$, $\phi = 0.01$, and Le $= 20$.

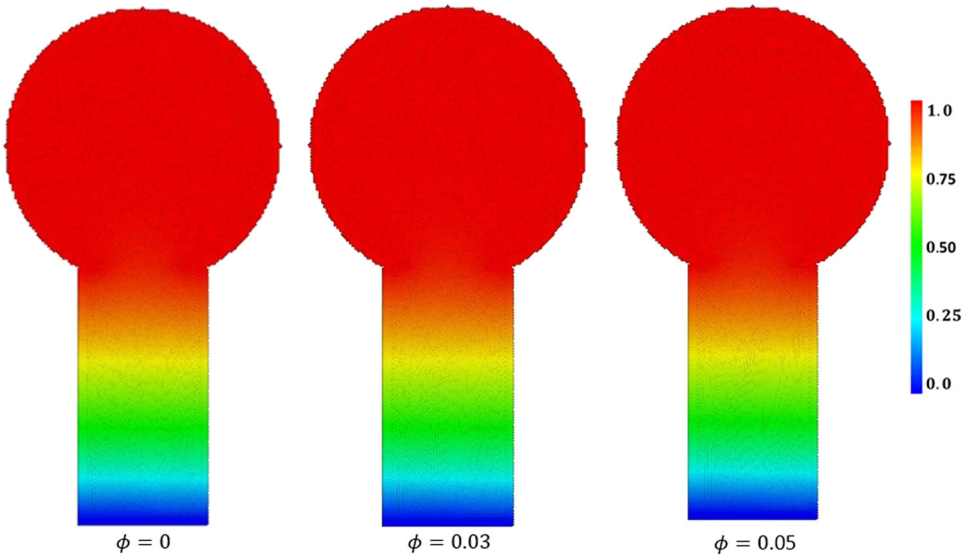


**Figure 9:** Variation of $\phi$ on temperature at $N = 1$, $\eta_1 = \eta_2 = 1.5$, $R_c = 0.1$, Da $= 10^{-3}$, Ra $= 10^4$, and Le $= 20$.

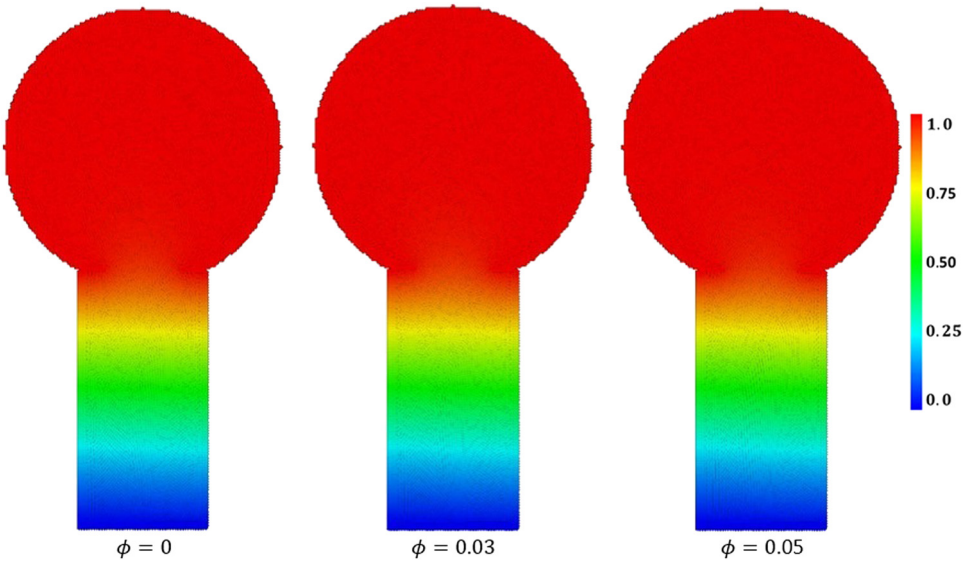


**Figure 10:** Variation of $\phi$ on concentration at $N = 1$, $\eta_1 = \eta_2 = 1.5$, $R_c = 0.1$, Da $= 10^{-3}$, Ra $= 10^4$, and Le $= 20$.

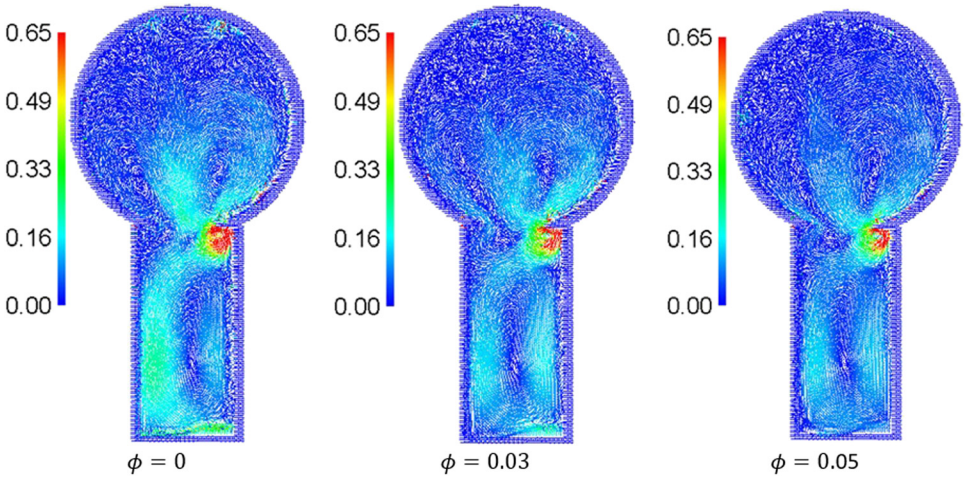


**Figure 11:** Variation of $\phi$ on velocity fields at $N = 1$, $\eta_1 = \eta_2 = 1.5$, $R_c = 0.1$, Da $= 10^{-3}$, Ra $= 10^4$, and Le $= 20$.

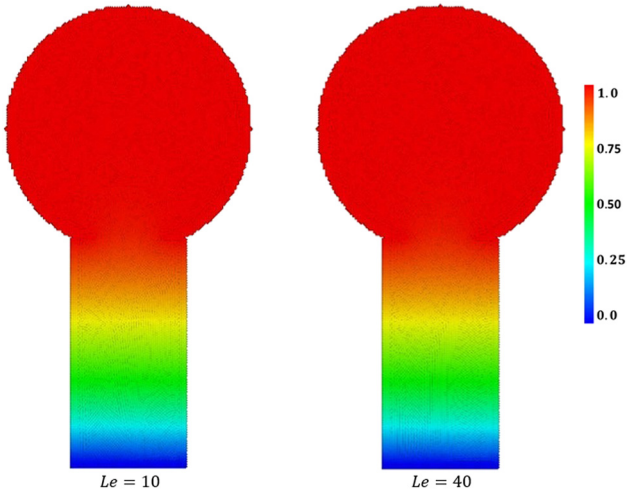


**Figure 12:** Variation of Le on temperature at $N = 1$, $\eta_1 = \eta_2 = 1.5$, $L_h = 0.25$, $R_c = 0.1$, Da $= 10^{-3}$, Ra $= 10^4$, and $\phi = 0.01$.

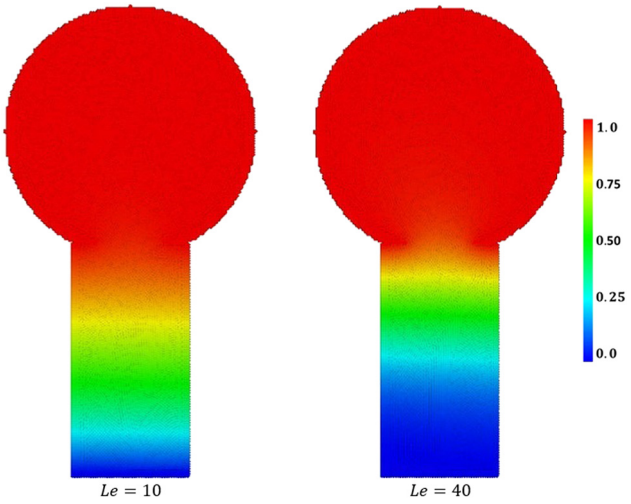


**Figure 13:** Variation of Le on concentration at $N = 1$, $L_h = 0.25$, $\eta_1 = \eta_2 = 1.5$, $R_c = 0.1$, Da $= 10^{-3}$, Ra $= 10^4$, and $\phi = 0.01$.

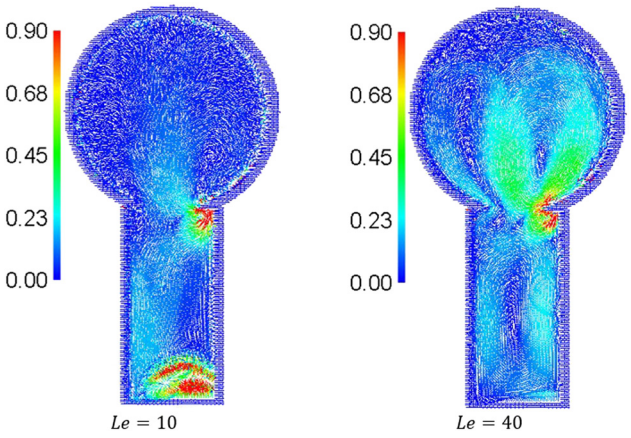


**Figure 14:** Variation of Le on velocity fields at $N = 1$, $L_h = 0.25$, $\eta_1 = \eta_2 = 1.5$, $R_c = 0.1$, Da $= 10^{-3}$, Ra $= 10^4$, and $\phi = 0.01$.

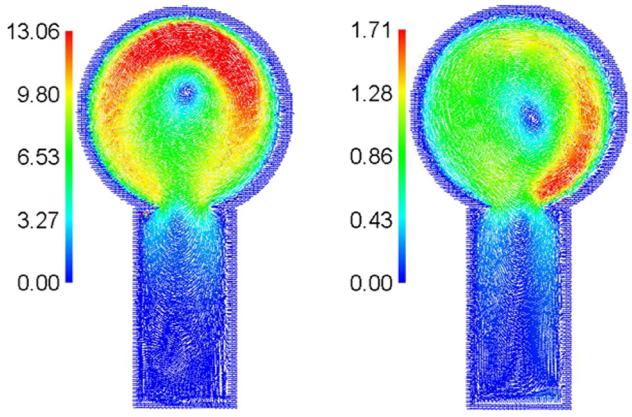


**Figure 17:** Variation of wall-boundary conditions on velocity fields at $N = 1$, $L_h = 0.25$, $\eta_1 = \eta_2 = 1.5$, $R_c = 0.1$, Da $= 10^{-3}$, Ra $= 10^4$, $\phi = 0.01$, and Le $= 20$.

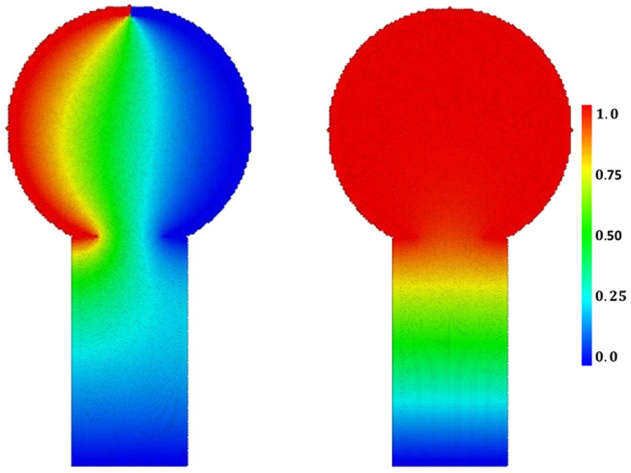


**Figure 15:** Variation of wall-boundary conditions on temperature at $N = 1$, $\eta_1 = \eta_2 = 1.5$, $L_h = 0.25$, $R_c = 0.1$, Da $= 10^{-3}$, Ra $= 10^4$, $\phi = 0.01$, and Le $= 20$.

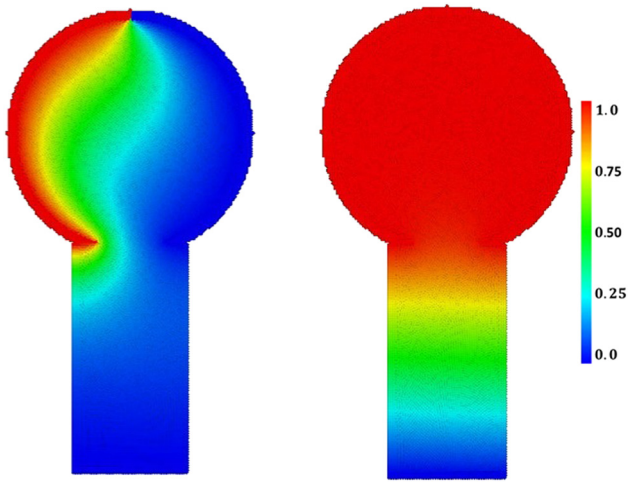


**Figure 16:** Variation of wall-boundary conditions on concentration at $N = 1$, $L_h = 0.25$, $\eta_1 = \eta_2 = 1.5$, $R_c = 0.1$, Da $= 10^{-3}$, Ra $= 10^4$, $\phi = 0.01$, $\varepsilon = 0.6$, and Le $= 20$.

Darcy parameter on the features of heat/mass transport and nanofluid velocity are conducted.

The accompanying points are the principal discoveries of the current study:

- A homogeneous porous medium reduces the temperature and concentration distributions as well as the velocity field compared to a heterogeneous porous medium.
- As a Darcy parameter signifies a porous resistance for nanofluid flow, the velocity field is decreasing as Darcy parameter decreases.
- An increase in Rayleigh number with higher value of a buoyancy ratio are augmenting heat/mass transport as well as a nanofluid velocity.
- An increase in solid volume fraction decelerates the nanofluid motion due to extra viscosity a nanofluid.
- Variations in wall boundary conditions change the transmission of heat/mass within a combined cavity.
- A homogeneous porous medium supports stable nanofluid movements inside a combined cavity compared to a heterogeneous porous medium.

## Nomenclature

| | |
|---|---|
| $C$ | mass concentration |
| Da | Darcy parameter |
| Pr | Prandtl number |
| $U$, $V$ | dimensionless velocities |
| $K_B$ | Boltamann's coefficient |
| $C_p$ | heat capacity |
| $x$, $y$ | dimensional Cartesian coordinates |
| $P$ | dimensionless pressure |
| $k$ | thermal conductivity |
| Ra | Rayleigh number |

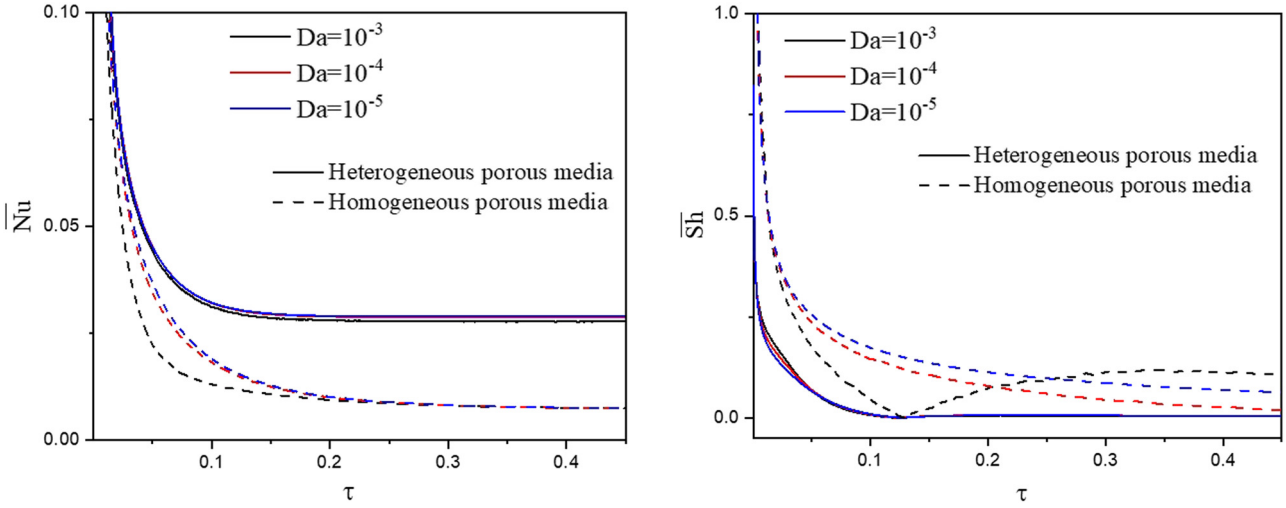


**Figure 18:** Average Nusselt $\overline{\mathrm{Nu}}$ & Sherwood $\overline{\mathrm{Sh}}$ numbers a long a circular cylinder wall below the effects of Da with two levels of porous media at $N = 2$, $\mathrm{Ra} = 10^4$, $\phi = 0.01$, $\varepsilon = 0.6$ and $\mathrm{Le} = 20$.

| | |
|---|---|
| $W$ | kernel function |
| $t$ | dimensional time |
| $K_0$ | permeability |
| $X$, $Y$ | dimensionless Cartesian coordinates |
| $u_B$ | Brownian velocity |
| $T$ | dimensional temperature |
| $L$ | height of a rectangular cavity |
| $u$, $v$ | dimensional velocities |
| Greek symbols | |
| $\varepsilon$ | porosity |
| $\eta_1$ | change rate of $\ln(K)$ in $X$ |
| $\eta_2$ | change rate of $\ln(K)$ in $Y$ |
| $\Phi$ | dimensionless mass |
| $\mu$ | dynamic viscosity |
| $\phi$ | solid volume fraction |
| $\tau$ | dimensionless time |
| $\rho$ | density |
| $\theta$ | dimensionless temperature |
| Subscripts | |
| $f$ | fluid |
| nf | Nanofluid |
| $p$ | porous medium |
| $c$ | cold |
| $h$ | hot |

**Acknowledgments:** The authors extend their appreciation to the Deanship of Scientific Research at King Khalid University, Abha, Saudi Arabia, for funding this work through the Research Group Project under Grant Number (RGP. 2/36/43). This research was funded by the Princess Nourah bint Abdulrahman University Researchers Supporting Project number (PNURSP2022R102), Princess Nourah bint Abdulrahman University, Riyadh, Saudi Arabia.

**Funding information:** This research was funded by the Deanship of Scientific Research at King Khalid University, Abha, Saudi Arabia, for funding this work through the Research Group Project under Grant Number (RGP. 2/36/43). This research was funded by the Princess Nourah Bint Abdulrahman University Researchers Supporting Project number (PNURSP2022R102), Princess Nourah bint Abdulrahman University, Riyadh, Saudi Arabia.

**Author contributions:** All authors have accepted responsibility for the entire content of this manuscript and approved its submission.

**Conflict of interest:** The authors state no conflict of interest.

**Data availability statement:** The data that support the findings of this study are available upon request from the first author (Abdelraheem M. Aly; E-mail: abdelreheam.abdallah@sci.svu.edu.eg).

## References

[1] Lewis RW, Morgan K, Thomas H, Seetharamu KN. The finite element method in heat transfer analysis. Hooken, New Jersey, U.S.: John Wiley and Sons; 1996.

[2] Lewis RW, Nithiarasu P, Seetharamu KN. Fundamentals of the finite element method for heat and fluid flow. New Jersey, U.S.: John Wiley and Sons; 2004.

[3] Nithiarasu P, Lewis RW, Seetharamu KN. Fundamentals of the finite element method for heat and mass transfer. Hooken, New Jersey, U.S.: John Wiley and Sons; 2016.
[4] Lai F, Kulacki F, Prasad V. Mixed convection in saturated porous media, in: Convective heat and mass transfer in porous media. Dordrecht, Holland: Springer; 1991. p. 225–87.
[5] Ingham DB, Pop I. Transport phenomena in porous media. Amsterdam: Elsevier; 1998.
[6] Nield DA, Bejan A, Nield-Bejan. Convection in porous media. Berlin, Germany: Springer; 2006.
[7] Vadász P. Emerging topics in heat and mass transfer in porous media: from bioengineering and microelectronics to nanotechnology. Berlin, Germany: Springer Science and Business Media; 2008.
[8] Vanaki SM, Ganesan P, Mohammed H. Numerical study of convective heat transfer of nanofluids: a review. Renew Sustain Energy Rev. 2016;54:1212–39.
[9] Nguyen MT, Aly AM, Lee S-W. Effect of a wavy interface on the natural convection of a nanofluid in a cavity with a partially layered porous medium using the ISPH method. Numer Heat Trans A Appl. 2017;72:68–88.
[10] Ataei-Dadavi I, Chakkingal M, Kenjeres S, Kleijn CR, Tummers MJ. Experiments on mixed convection in a vented differentially side-heated cavity filled with a coarse porous medium. Int J Heat Mass Transfer. 2020;149:119238.
[11] Nguyen TK, Soomro FA, Ali JA, Haq RU, Sheikholeslami M, Shafee A. Heat transfer of ethylene glycol-Fe3O4 nanofluid enclosed by curved porous cavity including electric field. Phys A Statist Mech Appl. 2020;550:123945.
[12] Selimefendigil F, Öztop HF. Magnetohydrodynamics forced convection of nanofluid in multi-layered U-shaped vented cavity with a porous region considering wall corrugation effects. Int Commun Heat Mass Transf. 2020;113:104551.
[13] Khan ZH, Makinde OD, Hamid M, Haq RU, Khan WA. Hydromagnetic flow of ferrofluid in an enclosed partially heated trapezoidal cavity filled with a porous medium. J Magnetism Magnetic Materials. 2020;499:166241.
[14] Raja MAZ, Rehman Khan MA, Mahmood T, Farooq U, Ishtiaq Chaudhary N. Design of bio-inspired computing technique for nanofluidics based on nonlinear Jeffery-Hamel flow equations. Canadian J Phys. 2016;94(5):474–89. doi: 10.1139/cjp-2015-0440.
[15] Raja MAZ, Khan Z, Zuhra S, Ishtiaq Chaudhary N, UllahKhan W, He Y, et al. Cattaneo-christov heat flux model of 3D hall current involving biconvection nanofluidic flow with Darcy-Forchheimer law effect: Backpropagation neural networks approach. Case Studies Thermal Eng. 2021;26:101168.
[16] Chamkha AJ, Ahmed SE. Unsteady MHD heat and mass transfer by mixed convection flow in the forward stagnation region of a rotating sphere at different wall conditions. Chem Eng Commun. 2012;199(1):122–41.
[17] Ahmed SE, Mansour MA, Mahdy A, Mohamed SS. Entropy generation due to double diffusive convective flow of Casson fluids over nonlinearity stretching sheets with slip conditions. Eng Sci Technol Int J. 2017;20(6):1553–62.
[18] Hussain S, Ahmed SE. Unsteady MHD forced convection over a backward facing step including a rotating cylinder utilizing Fe3O4-water ferrofluid. J Magnetism Magnetic Materials. 2019;484:356–66.
[19] Elshehabey HM, Raizah Z, Oztop HF, Ahmed SE. MHD natural convective flow of Fe3O4-H2O ferrofluids in an inclined partial open complex wavy walls ringed enclosures using non-linear Boussinesq approximation. Int J Mech Sci. 2020;170:105352.
[20] Armaghani T, Chamkha A, Rashad AM, Mansour MA. Inclined magneto: convection, internal heat, and entropy generation of nanofluid in an I-shaped cavity saturated with porous media. J Thermal Anal Calorimetry. 2020;142(6):2273–85.
[21] Ahmed SE, Mansour MA, Rashad AM, Salah T. MHD natural convection from two heating modes in fined triangular enclosures filled with porous media using nanofluids. J Thermal Anal Calorimetry. 2020;139(5):3133–49.
[22] Chamkha AJ, Armaghani T, Mansour MA, Rashad AM, Kargarsharifabad H. MHD Convection of an Al2O3-Cu/Water Hybrid Nanofluid in an Inclined Porous Cavity with Internal Heat Generation/Absorption. Iranian J Chemistry Chemical Eng (IJCCE). 2021;41(3):936–56.
[23] Reddy PBA, Salah T, Jakeer S, Mansour MA, Rashad AM. Entropy generation due to magneto-natural convection in a square enclosure with heated corners saturated porous medium using Cu/water nanofluid. Chin J Phys. 2022;77:1863–84.
[24] Ismael MA. Double-diffusive mixed convection in a composite porous enclosure with arc-shaped moving wall: tortuosity effect. J Porous Media. 2018;21(4):343–62.
[25] Ismael MA, Ghalib HS. Double diffusive natural convection in a partially layered cavity with inner solid conductive body. Scientia Iranica. 2018;25(5):2643–59.
[26] Kadhim HT, Jabbar FA, Rona A. Cu-Al2O3 hybrid nanofluid natural convection in an inclined enclosure with wavy walls partially layered by porous medium. Int J Mech Sci. 2020;186:105889.
[27] Sheikholeslami M, Shehzad SA, Li Z. Water based nanofluid free convection heat transfer in a three dimensional porous cavity with hot sphere obstacle in existence of Lorenz forces. Int J Heat Mass Transf. 2018;125:375–86.
[28] Seyyedi SM, Hashemi-Tilehnoee M, Sharifpur M. Impact of fusion temperature on hydrothermal features of flow within an annulus loaded with nanoencapsulated phase change materials (NEPCMs) during natural convection process. Math Probl Eng. 2021;2021:4276894.
[29] Seyyedi SM, Hashemi-Tilehnoee M, Sharifpur M. Effect of inclined magnetic field on the entropy generation in an annulus filled with NEPCM suspension. Math Probl Eng. 2021;2021:8103300.
[30] Hashemi-Tilehnoee M, Dogonchi AS, Seyyedi SM, Sharifpur M. Magneto-fluid dynamic and second law analysis in a hot porous cavity filled by nanofluid and nano-encapsulated phase change material suspension with different layout of cooling channels. J Energy Storage. 2020;31:101720.
[31] Seyyedi SM. On the entropy generation for a porous enclosure subject to a magnetic field: Different orientations of cardioid geometry. Int Commun Heat Mass Transf. 2020;116:104712.
[32] Aly Abdelraheem M. Natural convection of a nanofluid-filled circular enclosure partially saturated with a porous medium using ISPH method. Int J Numer Meth Heat Fluid Flow. 2020;30(11):4909–32.
[33] Aly AM, Raizah Z, Asai M. Natural convection from heated fin shapes in a nanofluid-filled porous cavity using incompressible smoothed particle hydrodynamics. Int J Numer Meth Heat Fluid Flow. 2019;29(12):4569–97.

[34] Aly AM, Raizah Z. Incompressible smoothed particle hydrodynamics simulation of natural convection in a nanofluid-filled complex wavy porous cavity with inner solid particles. Phys A Statist Mech Appl. 2020;537:122623.
[35] Raizah ZAS, Ahmed SE, Aly AM. ISPH simulations of natural convection flow in E-enclosure filled with a nanofluid including homogeneous/heterogeneous porous media and solid particles. Int J Heat Mass Transf. 2020;160:120153.
[36] Aly AM, Raizah ZAS. Incompressible smoothed particle hydrodynamics method for natural convection of a ferrofluid in a partially layered porous cavity containing a sinusoidal wave rod under the effect of a variable magnetic field. AIP Adv. 2019;9:105210.
[37] Aly AM, Raizah ZAS, Sheikholeslami M. Analysis of mixed convection in a sloshing porous cavity filled with a nanofluid using ISPH method. J Thermal Anal Calorimetry. 2020;139:1977–91.
[38] Raizah Z, El-Sapa S, Aly AM. ISPH simulations of thermosolutal convection in an annulus amongst an inner prismatic shape and outer cavity including three circular cylinders. Case Studies Thermal Eng. 2022;30:101736.
[39] Zhuang YJ, Zhu QY. Numerical study on combined buoyancy-Marangoni convection heat and mass transfer of power-law nanofluids in a cubic cavity filled with a heterogeneous porous medium. Int J Heat Fluid Flow. 2018;71:39–54.
[40] Corcione M. Empirical correlating equations for predicting the effective thermal conductivity and dynamic viscosity of nanofluids. Energy Conver Manag. 2011;52(1):789–93.
[41] Garoosi F, Bagheri GH, Talebi F. Numerical simulation of natural convection of nanofluids in a square cavity with several pairs of heaters and coolers (HACs) inside. Int J Heat Mass Transf. 2013;7:362–76.
[42] Bianco V, Manca O, Nardini S. S. Entropy generation analysis of turbulent convection flow of Al2O3ewater nanofluid in a circular tube subjected to constant wall heat flux. Energy Convers Manag, 2014;7:306–14.
[43] Kim BS, Lee DS, Ha MY, Yoon HS. A numerical study of natural convection in a square enclosure with a circular cylinder at different vertical locations, Int J Heat Mass Transf. 2008;51(7):1888–906.